Revised Manuscript- clean version [word file]

Click here to view linked References

The removal preference of Fe(III), Fe(II), and in situ Fe(III) in coagulation when treating NOM and TC

Qingyun Song [a, b, c], Bingqian Yang [b, c], Nigel Graham [d], Muhammad Saboor Siddique [b, c], Shian Song [b], Wenzheng Yu [b*]

[a] School of Environment, Henan Key Laboratory for Environment Pollution Control, Key Laboratory of Yellow River and Huai River Water Environment Pollution Control, Ministry of Education, Henan Province's International Joint Laboratory on Key Techniques in Water Treatment, Henan Normal University, Xinxiang, Henan 453007, China

[b] State Key Laboratory of Environmental Aquatic Chemistry, Research Center for Eco-Environmental Sciences, Chinese Academy of Sciences, Beijing 100085, China (wzyu@rcees.ac.cn)

[c] University of Chinese Academy of Sciences, Beijing 100049, China

[d] Department of Civil and Environmental Engineering, Imperial College London, South Kensington Campus, London SW7 2AZ, United Kingdom (n.graham@imperial.ac.uk)

Abstract

Tetracyclines (TCs) are a representative class of emerging organic pollutants. Their presence may affect the coagulation process commonly used in water treatment units. Fe salts are widely employed as coagulants in the coagulation process. However, there are few systematic studies of Fe(III), Fe(II), and in situ Fe(III) (oxide-assisted Fe(II) coagulation) for the treatment of natural organics (NOMs) in the presence or absence of tetracycline (TC). In this study, the coagulation process and performance of Fe(III), Fe(II) and in-situ Fe(III) generated by the oxide of potassium persulfate (PS) for the removal of humic acid (HA), NOM, NOM with TC were systematically studied. The flocculation index showed that the presence of TC lagged the floc growth. It was due to the reaction of TC with Fe, hindering the hydrolysis, aggregation and precipitation of Fe to form flocs. The removal performance evaluated by the EEM, SEC and LC-MS suggested the removal preference of Fe(III) and Fe(II) was NOM and TC, respectively. And the in-situ Fe(III) was superior than Fe(III) and Fe(II) in removing NOM and TC. It was attributed to the free radical oxidation by PS and the coagulation through in-situ Fe(III). The concentration of PS determined which of them was the main reason responsible for the enhanced organics removal. The PS at the concentration of 0.02 mM was the key point. The oxidation of organics by the free radicals dominated the enhance removal of organics when PS concentration was lower than 0.02mM. Otherwise, it was the coagulation of the in-situ Fe(III) responsible for the enhanced removal of organics. The results of floc characterization by TEM, SEM and FTIR further indicated that the in-situ Fe(III) retained higher proportion organics with the increased concentration of PS. This study provides information on which Fe salt coagulant to choose for the treatment of TC-contaminated water and the insights of the interactions fate of Fe flocs with NOM and TC from the perspective of coagulation in natural environments.

Key words: Coagulation; Fe(III); Fe(II); in-situ Fe(III); NOM; TC

1. Introduction

Coagulation is widely employed in water treatment due to its low cost and easy operation[1, 2]. The coagulants in this process undergo fast hydrolysis, polymerization, and precipitation[3]. Eventually, the precipitation products named flocs can achieve the separation of contaminants from the liquid phase to the solid phase[4]. The active sites (-OH and -OH_2) are the key for floc aggregation[5]. The separation usually is the result of a combination of actions such as charge neutralization, adsorption, and sweep flocculation during the floc growth process[6]. Due to the floc dynamic growth, the newly exposed floc surfaces can influence the interactions of flocs and contaminants and thereby the performance[7, 8].

Fe(III) and Fe(II) salts are commonly used coagulants for removing organic matter and phosphate[9]. Among them, in-situ Fe(III) generated from Fe(II) oxidation performs better at certain conditions. It was found that in-situ Fe(III) naturally formed from Fe(II) is more effective than that of Fe(III) on the removal of phosphate[10]. In addition, oxides enhanced coagulation has been developing due to the higher requirement on water quality and safety[11, 12]. In-situ Fe(III) accelerated formed from Fe(II) by the oxidation of potassium permanganate achieved enhanced removal of natural organic matter (NOM)[13]. Also, it kept effective removal of phosphate in natural waters when comparing to that of Fe(II) and Fe(III)[10]. Additionally, coagulation achieved by the interactions of flocs and contaminants shows that contaminants play an equally important role in coagulation as flocs[3, 14]. The presence and the types of contaminants influence the microstructure of the formed flocs and thereby their performance[3, 14].

Emerging organic contaminants, initially invented for serving human society, have been entered into aqueous environment at detectable concentrations and have been posing environmental risks[15, 16]. Typical tetracyclines (TCs) in environment put deleterious impact the ecological and human health[17, 18]. They can induce biological genetic

resistance[19], and can generate disinfection by-products[20]. They are inevitably able to interact with NOM in natural waters[21]. The photolysis of TC in aquatic environment can be hindered by NOM, resulted from comprehensive function of multiple factors[22]. In addition, it was confirmed that electron transfer occurs between in Fe(II) bearing clay minerals and TC in natural environment[23]. Therefore, it is reasonable to interfere that the presence of TC and its interactions with NOM and Fe coagulants can influence the formation of Fe flocs and thereby the performance of coagulation. However, it remains unclear the floc growth behavior pattern of Fe(III), Fe(II), and in-situ Fe(III) towards NOM in the absence and presence of TC. Correspondingly, whether there are commonalities and differences between above Fe for the removal of NOM and TC remains to be explored.

Hence, the objectives of this study were to investigate: (i) the influence of TC on the floc growth pattern of Fe(III), Fe(II), and in-situ Fe(III), (ii) the preference of Fe(III), Fe(II), and in-situ Fe(III) towards the removal of NOM and TC, and (iii) the mechanism. It should be noted that in-situ Fe(III) in this study was obtained from the oxidation of Fe(II) by an oxide (potassium persulfate, (PS)). PS is an oxidizing persulfate[24]. However, it has a low oxidation efficiency[25]. Fe-based substances can effectively activate PS and decompose pollutants[26]. PS has been used in coagulation treatment processes[27, 28]. The reaction of Fe(II) with PS can produce Fe(III)[29]. Due to PS was also used in Fe(III) coagulation for comparison, for better differentiation, Fe(III)-PS and Fe(II)-PS are used in the following text. As with the conclusions on phosphorus removal by Fe coagulants, it was expected that valuable conclusions can be obtained through this experiment, which can provide a reference for coagulation treatment by Fe salts of tetracycline-containing contaminated water. Additionally, considering the ubiquity of Fe and the large amount of TC in natural environment, this study could also provide the insights of the interactions fate of Fe flocs with NOM and TC from the perspective of coagulation.

2. Materials and methods

2.1. Chemicals

All reagents were analytical, or higher, grade and used without further purification. Humic acid sodium salt (HA) and tetracycline hydrochloride (TC) ($C_{22}H_{24}N_2O_8$•HCl, >99%) were purchased from Sigma-Aldrich (St. Louis, MO, USA). Ferric sulfate ($Fe_2(SO_4)_3$, 99%), ferrous sulfate (Fe_2SO_4•$7H_2O_2$, 99%), potassium persulfate ($K_2S_2O_8$, 99%), hydrochloric acid (HCl, 36.0~38.0%), sodium hydroxide (NaOH, ≥96.0%) and sodium bicarbonate ($NaHCO_3$, ≥99.5%) were purchased from Sinopharm Chemical Reagent Co., Ltd. (Shanghai, China). Deionized water (DI) (>18 mΩ·cm, Milli-Q system, USA) was used throughout for solution preparation.

2.2. Experimental process

The coagulation experiments were performed in the following solutions: 5 mM $NaHCO_3$, HA with 5 mM $NaHCO_3$, a surface water, and the TC-contaminated surface water. The HA stock solution (10 g/L) was prepared according to the method reported by Li et al. [30], briefly: 1 g sodium humic acid and 0.1 g NaOH were added to 100 mL DI, and the solution mixed by magnetic stirrer for 24 h. A specific volume of HA stock solution was diluted with 5 mM $NaHCO_3$ to obtain a HA solution of a certain concentration. The total organic carbon (TOC) of HA used in this study was 1.32 mg/L. The pH of $NaHCO_3$ and HA solutions were adjusted to pH 8.0 by adding 0.1M HCl or/and NaOH to simulate that of the surface water. The surface water samples were obtained from the Jingmi surface water (JM) in Beijing, China. The water samples were filtered by 0.45 mm membrane prior to use in order to remove particulate matter and biopolymers. The water samples were stored in the dark at 4 ºC before use. The TC-contaminated surface water (JT) was achieved by adding the

required volume of TC to the surface water with agitation. The TOC of TC was 0.94 mg/L. The basic water quality of HA, JM and JT are shown in Supplementary material (Table S1).

The coagulation experiments were all carried out at room temperature (25 ± 1 ºC), using a multiple stirrer, flocculator (MY3000-2N, Wuhan Meiyu, China). The coagulation 'jar test' procedure was conducted as follows: firstly, rapid stirring at a speed of 200 rpm for 1 min to achieve good mixing, and then stirring at 50 rpm for 30 min for the growth of the flocs. The floc growth was continuously monitored by a Photometric Dispersion Analyzer (PDA2000, Rank Brothers Ltd, UK). This equipment can represent the floc growth as the variation in flocculation index with time. The flocculation index is the ratio of the root mean square, to the average, transmitted light intensity [3], and is positively correlated with the size of flocs. The Fe coagulants and PS oxidant were introduced into previously prepared solutions, and then the coagulation process was started and continuously monitored by the PDA instrument. After the test, the flocs were removed from the solution, air dried and stored for characterization and analysis.

2.3. Analytical methods

The excitation and emission matrix (EEM) fluorescence spectra of water samples were analyzed by EEM fluorescence spectroscopy (F-4600, HITACHI, Japan). Size exclusion chromatography (SEC) involving an HPLC system (Perkin Elmer, USA), a BIOSEP-SEC-S3000 column (Phenomenex, UK) (7.8 mm×300 mm), and a Security Guard column fixed with a GFC-3000 disc 4mm (ID), was used to determine the molecular weight distribution of UV sensitive substances. The mobile phase was 10 mM sodium acetate solution. 100 μL water sample was injected and detected at a wavelength of 254 nm. In addition, the UV-visible absorbance spectra of the water samples were obtained using a UV–visible analyzer (UV-2600, Shimadzu, Japan) with a 1 cm path length quartz cuvette, and a scanning range of

200 nm to 800 nm. The TOC of water samples were measured through a TOC analyzer (TOC-VCPH, Shimadzu, Japan). The radicals generated from Fe(II)-activated PS were captured by employing 5-dimethyl-1-pyrroline N-oxide (DMPO, D2362, TCI, Japan) and then detected by electron paramagnetic resonance (EPR) spectrometry (A300, BRUKER, USA) to obtain the radicals' electron spin resonance (ESR) spectra. TC and its transformation products were identified using an ultra-performance liquid chromatograph coupled with Q-Exactive Orbitrap mass spectrometer (UPLC/Q-Exactive Orbitrap MS, TM Ultimate 3000, Thermo Scientific).

2.4. Flocs characterization

The morphology of the dried flocs was analyzed by field emission scanning electron microscopy (FE-SEM, 166 Hitachi SU8020, Japan) after gold coating pretreatment. Furthermore, the flocs' morphology and lattice fringes were captured by field emission transmission electron microscopy (TEM, Tecnai G2 F30, FEI, US). The functional groups of flocs were analyzed through Fourier transform infrared spectroscopy (FT-IR, Spectrum 400, PerkinElmer, USA).

3. Results and discussion

3.1. Floc growth

The flocculation index provided the information about floc initial rate of increase and the maximum/equilibrium value[3]. Figure S1 shows that PS had slight influence on Fe(III) floc growth time and size in $NaHCO_3$ without the disturbance of organics, suggesting the lower reactivity of Fe(III) towards PS. Nevertheless, the introduction of HA hindered the flocs of Fe(III) formed with/without PS. It indicated the complete occupation of Fe(III) active sites by HA, resulting in the failure of hydrolysis and aggregation of Fe(III). However, the

168 aggregation of Fe(III) nanoparticles in NOM was achieved, owing to the difference of HA
169 and NOM in JM. Whereas, Figure 1 shows that Fe(II) grew slower and larger than that of
170 Fe(III) in $NaHCO_3$, suggesting the faster aggregation and compacter structure of Fe(III) than
171 that of Fe(II). It was due to that Fe(III) may possess more active sites of oxygen-containing
172 groups[30, 31]. They facilitated Fe(III) to bond with each other, forming compacter
173 structure[31]. And the solubility of Fe(III) is lower than that of Fe(II), resulting the faster
174 precipitation of Fe(III)[30]. Nevertheless, Fe(II) differed from Fe(III) that it formed flocs
175 with the presence of HA. According to the performance above, it was inferred that the less
176 active sites on Fe(II) facilitated their aggregation instead of combining with HA, resulting in
177 the growth of larger and looser precipitates with lower efficiency on HA removal[9]. Similar
178 results can be obtained from NOM (JM) and JT. However, the maximum/equilibrium value of
179 Fe(II) flocs in $NaHCO_3$ was reduced with the addition of PS of increasing concentrations.
180 The reduced size of Fe(II) was probably due to that the oxidation of Fe(II) to Fe(III)[9, 10,
181 30], and the size of Fe(III) was smaller[9, 10]. In the scenarios of JM and JT, similar
182 phenomenon can be observed that the floc size decreased with the addition of PS, which can
183 be explained by the same reasons. It should be noted that the flocculation index values of the
184 Fe(II) with 0.01 mM PS in HA and JM were slightly higher than that of Fe(II). It was due to
185 the fluctuations in the flocculation index value as illustrated in Figure 1. PDA monitoring of
186 floc size was achieved by repeatedly pumping the continuously growing floc by the pump,
187 which can lead to fluctuations in floc size. In addition, it can be found that the flocs grew
188 faster in JM and JT with the addition of PS, suggesting the faster oxidation of Fe(II) to Fe(III)
189 in the real surface water[9, 10]. It may be attributed to the different components showing in
190 HA and JM, the components in JM accelerated the oxidation of Fe(II)[32]. Accordingly, the
191 faster oxidation of Fe(II) to Fe(III) in JM can explain the reason of the same floc size in JM
192 with the increasing PS. The flocs were formed from the Fe(III) produced by the oxidation of

193 Fe(II)[13]. Besides, it can be found that the floc growth was lagged by the presence of TC. It
194 indicated that the aggregation of Fe flocs was hindered by TC. It was due to that Fe(III) and
195 Fe(II) may be consumed by their reaction with TC[33]. Nevertheless, all the floc size follows
196 the order of 'Fe(III) < Fe(II)-PS < Fe(II)'. The different floc variation of Fe(III) and Fe(II)
197 over time indicated their difference on microstructures[9], which was confirmed by the
198 characterization results.

199 ***Figure 1***

200

201 **3.2. Organics removal**

202 EEM was used for evaluating the performance of Fe coagulants on representative
203 organic matter of HA (Figure S2-7), NOM (JM) (Figure S9-11), and TC with NOM (JT)
204 (Figure S12, S13). To better comparing the EEM results, each EEM was divided into five
205 areas and then the intensity of every area was calculated. Figure 2(a) shows that the total
206 fluorescence intensities of removed substances from HA were slightly decreased by PS alone.
207 The total intensity of the removed substance follows the order of 'Fe(II) < Fe(III) < Fe(II)-PS
208 ≈ Fe(III)-PS', suggesting the superiority of Fe(III) on NOM removal with or without PS.
209 However, it can be found that the overall best performance was almost achieved in 2 minutes
210 from the time scale. Nevertheless, the removal efficiencies of Fe on corresponding five
211 substances were varying with time, suggesting the organic matter has been simultaneously
212 adsorbed and released during the growth of Fe flocs by hydrolysis, polymerization and
213 aggregation[34]. The presence of PS further influenced the removal tendency of coagulants
214 on corresponding substances in different times. PS can be activated by dissolved Fe and Fe
215 precipitates[7]. Therefore, the hydrolysis and aggregation of Fe to form flocs was affected by
216 PS, affecting the interactions of Fe and NOM. The influence of PS concentrations was also
217 studied (Figure S7, S8). The intensities of the removed substances and the removal

efficiencies of Fe increased as PS concentrations. Similar results of JM and JT can be obtained from Figure 2(b, c). However, the removal performance of Fe in JT follows the order of 'Fe(III) < Fe(II) < Fe(III)-PS < Fe(II)-PS', indicating the preference of Fe(II) on TC removal. Previous studies have found that the dissolved Fe interacted with TC through adsorption and complexation[33, 35, 36]. TC provided electrons to Fe(III), inducing the production of TC products and Fe(II). However, Fe(II) with one more electron produced extra radicals than that of Fe(III), contributing to TC transformation. And Fe precipitates (Fe flocs) coordinated to TC by the surface hydroxyl functional groups[37-39]. The redox reaction has been confirmed in the interactions of dissolved Fe and Fe precipitates[23, 33]. In addition, by comparing the efficiency improved by PS, it can be found that increasing PS concentrations was more effective in improving the removal of NOM by Fe(II). Based on the superiority of Fe(III) in the removal of NOM, it was mainly due to the formation of Fe(III) after the oxidation of Fe(II) by PS, and then the coagulation of Fe(III) was more conducive to the enhanced removal NOM. Whereas, PS was more effective in improving the removal of TC by Fe(III). Similarly, it was mainly due to the reaction of PS towards Fe(III) and Fe(III) flocs, which produced radicals and Fe(II) for TC removal.

Figure 2

The SEC results provided information about molecular weight distributions of organic matter after treatment (Figure S14). Their integral areas and corresponding removal efficiencies were calculated (Figure S15, Figure 3). It shows that the removal efficiency increased as molecular weight and coagulation time (Figure 3(a)). It was due to that the large molecular weight substance of higher hydrophobicity was more easily removed by coagulation [40, 41]. In addition, it suggested that the decreased EEM fluorescence intensities were attributed to their removal. Similar results can be obtained from JM and JT (Figure 3(b,

c1)). The different results of JT' EEM and SEC were due to that SEC provides information about NOM instead of TC. Hence, the UV375 representing the results of TC in JT were measured[7], which supported the EEM results of JT (Figure 3(c1)). In addition, it can be found that the floc growth over time influenced the reaction of flocs and organic matter. PS put more impact on removing low molecular weight organic during floc formation (Figure 3(d1, d2)). ESR determined that the radicals were involved in PS assisted-Fe coagulation (Figure 4a). And our previous study has found that Fe flocs can activate PS to generate radicals[7]. Therefore, it was radicals generated from PS enhanced the removal of low molecular weight organics as compared to that of Fe coagulation in the absence of PS. Whereas, the variation of PS concentrations had different influence on Fe(III) and Fe(II) when treating different molecular weight organic matter (Figure 3(d3,d4)). It can be found that the removal of low molecular weight organics by Fe(III) was higher than that of large molecular weight organics. It suggested that PS enhanced Fe(III) coagulation by the oxidation of organics. However, PS at the concentration of 0.02 mM was a turning point for Fe(II). When PS concentrations were less than 0.02 mM, a higher removal of lower molecular weight organics was achieved by Fe(II). The result of Fe(II) was similar to that of Fe(III) under this condition. Therefore, it can be explained by the same reason. It was radicals generated from PS activation by Fe(II) dominated the enhanced removal of NOM. When PS concentrations were higher than 0.02 mM, an opposite result was obtained that a higher removal of larger molecular weight organics was achieved by Fe(II), suggesting the main role of coagulation in enhancing the removal of NOM. It was probably attributed to the coagulation of Fe(III), which formed from Fe(II) by PS oxidation. Hence, PS improved Fe(II) coagulation by the oxidation of organics and Fe(II), and it was the concentration of PS determined whether the primary effect of enhanced NOM removal was oxidation or coagulation of organic matter.

268 ***Figure 3***

269

270 In addition, TC and its products in JM were further analyzed by LC-MS (Figure S16-
271 19). Their chemical information was provided (Table S2, S3). The results show the presence
272 of the products of TC in JM before the treatment, suggesting the influence of components in
273 JM. There were seven kinds of TC products, which were named P1, P2, P3, P4, P5, P6, and
274 P7. Their molecular weights were 452.9, 222.9, 162, 278.7, 249.9, 217.6 and 114. Therefore,
275 except that the mass molecular weight of P1 was higher than that of TC, the molecular weight
276 of P2 to P7 was lower than that of TC. Meanwhile, it can be found that the intensities of TC
277 (444.6) and its products with molecular mass of P1(452.9)[42], P2(222.9)[43],
278 P3(162)[44]were reduced by Fe without/with PS (Figure 4b, Table S2, Figure S16-19).
279 However, TC products with molecular mass of P4(278.7)[45], P5(249.9)[43], P6(217.6)[46],
280 P7(114)[46], were increased by Fe without/with PS (Figure 4b, Table S3, Figure S16-19). The
281 reduced/increased intensity follows the order of 'Fe(III) < Fe(II) < Fe(II)-PS' and 'Fe(III) >
282 Fe(II) > Fe(II)-PS', respectively (Figure 3b). The results further confirmed the preference of
283 Fe(II) coagulation when treating TC contaminated water with/without PS. It could be
284 explained by the same reasons.

285 ***Figure 4***

286

287 **3.3. Floc characterization**

288 To confirm the microstructure variation and difference of Fe flocs, characterization was
289 performed. Figure 5 provides information on the microstructure morphology and the
290 crystallinity of Fe flocs. It demonstrates the planar folds structure of Fe(II), co-existence of
291 the planar folds structure and nanoparticles structure of Fe(II)-PS, and nanoparticles structure
292 of Fe(III) through their TEM, HAADF, SEM images, respectively (Figure 5(a)). Therefore,

PS reacted with Fe(II) and contributed the transformation of plannar-like Fe(II) into nanoparticle Fe(III), reducing the floc size (flocculation index) of Fe(II). Furthermore, according to the high-resolution TEM, their resolved interplanar spacings were obtained to determine their mineral phases and thereby their crystallinity. The resolved interplanar spacings of Fe(II) were 3.12 Å, 2.98 Å, 2.47 Å, corresponding to the lattice planes of (012), (021) and (020) of lepidocrocite, respectively. Similarly, the resolved interplanar spacings of Fe(II)-PS were 3.41 Å, 2.56 Å, 2.28 Å, and coincided well to the (012), (020) and (004) lattice planes of six-line ferrihydrite. Lastly, the resolved interplanar spacings of Fe(III) were 3.41 Å, 2.47 Å, 2.56 Å, which corresponded to (012), (021) and (020) lattice planes of six-line ferrihydrite, respectively. Therefore, the crystallinity of the flocs follows the order of 'Fe(III) < Fe(II)-PS < Fe(II)'. It is their microstructural arrangement difference caused their different performance on organics removal, suggesting the high degree of disorder of the floc facilitated the removal of organics.

Figure 5

Also, FTIR characterization was performed to acquire information about their difference in functional groups. In the absence of organic matter (Figure 6(a)), the observed characteristic peaks at 464 cm^{-1}, and 700 cm^{-1} were Fe-O bending vibration[9]. The higher strength of Fe(II) than Fe(III) at the peaks confirmed the higher crystallization of Fe(II) flocs than Fe(III) flocs. With the introduction of organic matter, the characteristic peaks of HA and JM were determined in Fe flocs. For HA, the peaks of HA showed in the flocs at the wavelength of 1053 cm^{-1} (C-O bond)[47], 1375 cm^{-1} (COO- stretch vibration), 1574 cm^{-1} (C=C vibration) (Figure 6(b))[48]. For JM, the peaks of NOM belong to JM at 1015 cm^{-1} (C-O-C) can be found in Fe flocs (Figure 6(c))[49]. Similarly, the C=O group (1617 cm^{-1}), carboxylate COO^- (1581 cm^{-1}), C=C stretching (1450 cm^{-1}), C-N group (1249 cm^{-1}, 1224 cm^{-}

318 ^{1}) of TC peaks can be observed in Fe flocs (Figure S20(a))[23, 50]. It suggested that Fe
319 captured organic matter from the three different water samples. Furthermore, the 2D-COS
320 synchronous and asynchronous spectral results of the FTIR spectra were provided. The 2D-
321 COS map shows the overall effect of the oxide concentration on the determined FTIR peaks.
322 In the scenario of $NaHCO_3$, the highest auto-peak intensity was located in 400-800 cm^{-1},
323 corresponding to Fe-O variation. It suggested that the increased PS mainly influenced the floc
324 Fe-O bening in the absence of organics, resulting in higher production of Fe-O bending. The
325 synchronous auto peak intensity of HA follows the order of 1574 cm^{-1} > 1375 cm^{-1}> 1053
326 cm^{-1}, suggesting the proportion of C=C group of organic matter in Fe flocs increased the most
327 as PS concentration increased. For JM and JT, the synchronous auto peak intensity showed
328 higher proportion of functional groups of organic matter than that of Fe as the increased PS
329 concentration in flocs (Figure 6(b) and Figure S20(b)). The synchronous map results
330 suggested that the increased PS concentration had a greater effect on organic matter. In
331 addition to the scenario of $NaHCO_3$, the synchronous map showed that all cross-peaks were
332 positive correlated (Figure 6(b). However, the asynchronous map of HA showed that
333 1375/1053, 1574/1053, and 1574/1375 at the axis of X/Y were negative (Figure 6(c).
334 According to Noda' rule (Text S1)[51], take 1375/1053 for example, the opposite signs of it
335 in synchronous and asynchronous maps indicated that the functional groups of organics at
336 1053 cm^{-1} (C-O bond) (the Y-axis) reacted earlier than the organic functional groups at 1375
337 cm^{-1} (COO- stretch vibration) (the X-axis) as the increase of PS concentration[51].
338 Nevertheless, for JM, the positive signs of 1015/796 in synchronous and asynchronous maps
339 suggested the functional groups (C-O-C) at 1015 cm^{-1} responded earlier than Fe-OH at 796
340 cm^{-1}[52]. In summary, more intensive variations of functional groups of Fe and organic
341 matter in Fe flocs occurred as the increased PS concentration. The increased PS concentration
342 had a greater effect on organic matter and resulted in higher retention of organic matter.

Figure 6

3.4. Mechanism

The removal performance results show that the preference of Fe(III) and Fe(II) was NOM and TC in the absence/presence of PS, respectively. The structure of the Fe(III) precipitates were small and less ordered spherical nanoparticles of larger specific area, resulting in more sites for NOM removal. Whereas, the structure of Fe(II) precipitates were crystalline flakes. The one more electron provided by Fe(II) and the higher crystallinity of the Fe(II) precipitates determined their higher reactivity towards TC, leading to the higher transformation and capture of TC. The introduction of PS enhanced the Fe performance on the removal of organics. It enhanced the performance of Fe(III) and Fe(II) by oxidation towards organics, and oxidation towards Fe(II) and organics, respectively. As for Fe(III), PS could be activated by Fe(III), resulting in the radical attack towards organics. In the case of Fe(II), according to the analysis of the performance and characterization of Fe(II), PS first reacted with Fe(II), and then affected the removal of organic matter through in-situ Fe(III) coagulation and radical attack. The concentration of PS determined whether the primary effect of improved organic removal was in-situ Fe(III) coagulation or radicals.

Figure 7

4. Conclusions

NOM is ubiquitous in surface waters. Emerging contaminants have also been detected in a variety of water environments. The presence of NOM and emerging contaminants can affect coagulation behavior and performance. A systematic study of Fe(III), Fe(II) and oxidatively generated in-situ Fe(III) to remove NOM and the mixtures of emerging pollutants and NOM through coagulation is helpful to understand the effects of NOM and its compounds with

emerging pollutants on Fe flocculation and Fe cycling in the natural environment.

This study investigated the performance of Fe(III), Fe(II) and oxidatively generated in-situ Fe(III) when treating NOM and representative emerging contaminant of TC. The removal preference of Fe(III) and Fe(II) was NOM and TC, respectively. The in-situ Fe(III) produced by PS oxidation improved the removal of NOM and TC. The improved effect was achieved by free radical oxidation generated by PS and in-situ Fe(III) coagulation. The concentration of PS determined whether the dominant effect was oxidation or in-situ Fe(III) coagulation. This turning point concentration of PS was 0.02 mM. The conclusions of this study can provide reference information for the coagulation treatment of tetracycline-containing contaminated water by Fe salt.

Acknowledgments

This research was funded by the Beijing Natural Science Foundation (no. JQ21032) and the National Natural Science Foundation of China (Grants 52370184).

Author Contributions

Wenzheng Yu, Qingyun Song and Nigel Graham designed the experiments; Qingyun Song completed the main experiments and wrote the draft; Bingqian Yang, Muhammad Saboor Siddique and Shian Song provided help in the data analysis; Wenzheng Yu and Nigel Graham made the final revision to the manuscript.

Appendix A. Supplementary data

The Supplementary Material contains 1 Text, 4 Tables and 20 Figures.

The text is **Text S1.** Two-dimensional correlation spectroscopy (2D-COS).

The tables are as follows:

Table S1. Water quality characteristics of the water samples; **Table S2.** Chemical structures of TC and its reduced transformation products after treatment in JM surface water; **Table S3.**

393 Chemical structures of the increased TC transformation products after treatment in JM
394 surface water; **Table S4.** 2D-COS combined with the FTIR spectra: peak wavelength and the
395 signs of the cross peaks in synchronous (Syn) map and asynchronous (aSyn) map (shown in
396 bracket).
397 The figures are as follows:
398 **Figure S1.** Flocculation index variation of Fe(III) with PS in (a) $NaHCO_3$, HA, and
399 JM (PS: potassium persulfate, HA: humic acid, JM: Jingmi surface water); **Figure S2.** EEM
400 of (a) HA and HA after treating by PS of 0.1 mM and (b) substance removed from HA by PS
401 of 0.1 mM at different times (EEM: the excitation and emission matrix fluorescence spectra,
402 EEM partition I: protein I, II: protein II, III: fulvic acid, IV: microbial metabolites, V: humic
403 acid, HA: humic acid, PS: potassium persulfate); **Figure S3.** EEM of (a) HA after treating by
404 Fe(III) and (b) substance removed from HA by Fe(III) at different times (EEM: the excitation
405 and emission matrix fluorescence spectra, EEM partition I: protein I, II: protein II, III: fulvic
406 acid, IV: microbial metabolites, V: humic acid, HA: humic acid); **Figure S4.** EEM of (a) HA
407 after treating by Fe(II) and (b) substance removed from HA by Fe(II) at different times
408 (EEM: the excitation and emission matrix fluorescence spectra, EEM partition I: protein I, II:
409 protein II, III: fulvic acid, IV: microbial metabolites, V: humic acid, HA: humic acid); **Figure**
410 **S5.** EEM of (a) HA after treating by Fe(III) with PS of 0.1 mM, and (b) substance removed
411 from HA by Fe(III) with PS of 0.1 mM at different times (EEM: the excitation and emission
412 matrix fluorescence spectra, EEM partition I: protein I, II: protein II, III: fulvic acid, IV:
413 microbial metabolites, V: humic acid, HA: humic acid, PS: potassium persulfate); **Figure S6.**
414 EEM of (a) HA after treating by Fe(II) with PS of 0.1 mM, and (b) substance removed from
415 HA by Fe(II) with PS of 0.1 mM at different times (EEM: the excitation and emission matrix
416 fluorescence spectra, EEM partition I: protein I, II: protein II, III: fulvic acid, IV: microbial
417 metabolites, V: humic acid, HA: humic acid, PS: potassium persulfate); **Figure S7.** EEM of

(a) HA after treating by Fe(III) with PS of different concentrations, and (b) substance removed from HA by Fe(II) with PS of different concentrations (EEM: the excitation and emission matrix fluorescence spectra, EEM partition I: protein I, II: protein II, III: fulvic acid, IV: microbial metabolites, V: humic acid, HA: humic acid, PS: potassium persulfate); **Figure S8.** (a) The intensity of removed substance and (b) removal efficiency of HA, calculated from EEM (HA: humic acid, EEM: the excitation and emission matrix fluorescence spectra, EEM partition I: protein I, II: protein II, III: fulvic acid, IV: microbial metabolites, V: humic acid, PS: potassium persulfate); **Figure S9.** EEM of (a) JM and JM after treating by Fe(II) with PS of various concentrations, and (b) substance removed from JM by Fe(II) with PS of various concentrations (EEM: the excitation and emission matrix fluorescence spectra, EEM partition I: protein I, II: protein II, III: fulvic acid, IV: microbial metabolites, V: humic acid, JM: Jingmi surface water, PS: potassium persulfate); **Figure S10.** EEM of (a) JM after treating by Fe(II) with PS of various concentrations, and (b) substance removed from JM by Fe(II) with PS of various concentrations (EEM: the excitation and emission matrix fluorescence spectra, EEM partition I: protein I, II: protein II, III: fulvic acid, IV: microbial metabolites, V: humic acid, JM: Jingmi surface water, PS: potassium persulfate); **Figure S11.** EEM of (a) JM after treating by Fe(II) with PS of 0.1 mM, and (b) substance removed from HA by Fe(II) with PS of various concentrations (EEM: the excitation and emission matrix fluorescence spectra, EEM partition I: protein I, II: protein II, III: fulvic acid, IV: microbial metabolites, V: humic acid, JM: Jingmi surface water, PS: potassium persulfate); **Figure S12.** EEM of (a) JT and JT after treating by PS of various concentrations, (b) Fe(III) with PS of various concentrations and (c) Fe(II) with PS of various concentrations (EEM: the excitation and emission matrix fluorescence spectra, EEM partition I: protein I, II: protein II, III: fulvic acid, IV: microbial metabolites, V: humic acid, JT: Jingmi surface water with tetracycline hydrochloride, PS: potassium persulfate); **Figure S13.** EEM of (a) substances removed from JT by PS of various

443 concentrations, (b) Fe(III) with PS of various concentrations and (c) Fe(II) with PS of various
444 concentrations (EEM: the excitation and emission matrix fluorescence spectra, EEM partition
445 I: protein I, II: protein II, III: fulvic acid, IV: microbial metabolites, V: humic acid, JT: Jingmi
446 surface water with tetracycline hydrochloride, PS: potassium persulfate); **Figure S14.** SEC of
447 (a) HA, (b) JM and (c) JT (SEC: size exclusion chromatography, HA: humic acid, JM: Jingmi
448 surface water, JT: JM with tetracycline hydrochloride, SEC peak of HA: I(7052-50000),
449 II(5359-7052), III(3547-5359), peak of JM: I (5648-13145), II(3811-5648), peak of JT:
450 I(3031-6773), II(2061-3031), PS: potassium persulfate); **Figure S15.** Integral area of (a) HA,
451 (b) JM and (c) JT, calculated from SEC, (d) UV absorbance of JT, (e) UV absorbance of JT at
452 375 nm (HA: humic acid, JM: Jingmi surface water, JT: JM with tetracycline hydrochloride,
453 SEC: size exclusion chromatography, PS: potassium persulfate); **Figure S16.** (a) TIC of JT,
454 (b) LC-MS of JT (TIC: total ion chromatogram, JT: Jingmi surface water with tetracycline
455 hydrochloride, LC-MS: liquid chromatography-tandem mass spectrometry); **Figure S17.** (a)
456 TIC of JT after treating by Fe(III), (b) LC-MS of JT after treating by Fe(III) (TIC: total ion
457 chromatogram, JT: Jingmi surface water with tetracycline hydrochloride, LC-MS: liquid
458 chromatography-tandem mass spectrometry); **Figure S18.** (a) TIC of JT after treating by
459 Fe(II), (b) LC-MS of JT after treating by Fe(II) (TIC: total ion chromatogram, JT: Jingmi
460 surface water with tetracycline hydrochloride, LC-MS: liquid chromatography-tandem mass
461 spectrometry); **Figure S19.** (a) TIC of JT after treating by Fe(II) and 0.1 mM PS, (b) LC-MS
462 of JT after treating by Fe(II) and 0.1 mM PS (TIC: total ion chromatogram, JT: Jingmi
463 surface water with tetracycline hydrochloride, PS: potassium persulfate, LC-MS: liquid
464 chromatography-tandem mass spectrometry); **Figure S20.** FTIR spectra of flocs in (a) JT and
465 its (b) synchronous 2D-COS map, red colors represent positive intensities, blue colors
466 represent negative intensities (FTIR: Fourier transform infrared spectrometry, JT: Jingmi

surface water with tetracycline hydrochloride, 2D-COS: two-dimensional correlation spectroscopy, PS: potassium persulfate).

References

[1] B. Ren, K.A. Weitzel, X. Duan, M.N. Nadagouda, D.D. Dionysiou, A comprehensive review on algae removal and control by coagulation-based processes: mechanism, material, and application, Sep. Purif. Technol., 293 (2022) 121106.

[2] Y. Yue, G. An, L. Lin, H. Demissie, X. Yang, R. Jiao, D. Wang, Design and coagulation mechanism of a new functional composite coagulant in removing humic acid, Sep. Purif. Technol., 292 (2022) 121016.

[3] X.J. Zhang, N. Graham, L. Xu, W.Z. Yu, J. Gregory, The influence of small organic molecules on coagulation from the perspective of hydrolysis competition and crystallization, Environ. Sci. Tech., 55 (2021) 7456-7465.

[4] H. Chen, H. Xu, C. Zhong, M. Liu, L. Yang, J. He, Y. Sun, C. Zhao, D. Wang, Treatment of landfill leachate by coagulation: A review, Sci. Total Environ., 912 (2024) 169294.

[5] M. Wu, W. Yu, J. Qu, J. Gregory, The variation of flocs activity during floc breakage and aging, adsorbing phosphate, humic acid and clay particles, Water Res., 155 (2019) 131-141.

[6] A. H. Jagaba, A.H. Birniwa, A.K. Usman, N.D. Mu'azu, N.S.A. Yaro, U.B. Soja, K.J. Abioye, N.M.Y. Almahbashi, B.N.S. Al-dhawi, A. Noor, I.M. Lawal, Trend and current practices of coagulation-based hybrid systems for pulp and paper mill effluent treatment: mechanisms, optimization techniques and performance evaluation, J. Clean. Prod., 429 (2023) 139543.

[7] Y.H. Han, J.L. Wang, D.L. Xu, J.L. Song, H.S. Wang, X.W. Zhu, X.S. Luo, L. Yang, G.B. Li, H. Liang, Synergistic effect of potassium ferrate and ferrous iron for improving ultrafiltration performance in algae-laden water treatment, Water Res., 243 (2023).

[8] M. Qin, B. Lu, S. Feng, Z. Zhen, R. Chen, H. Liu, Role of exposed facets and surface OH groups in the Fenton-like reactivity of lepidocrocite catalyst, Chemosphere, 230 (2019) 286-293.

[9] X. Li, N.J.D. Graham, W.S. Deng, M.J. Liu, T. Liu, W.Z. Yu, Structural variation of precipitates formed by Fe(II) oxidation and impact on the retention of phosphate, Environ. Sci. Tech., 56 (2022) 4345-4355.

[10] B.Q. Yang, N. Graham, P. Liu, M.J. Liu, J. Gregory, W.Z. Yu, Atomic-level structural differences between Fe(III) coprecipitates generated by the addition of Fe(III) coagulants and by the oxidation of Fe(II) coagulants determine their coagulation behavior in phosphate and DOM removal, Environ. Sci. Tech.., 57 (2023) 12489-12500.

[11] Z.Y. Dong, Y.L. Lin, T. Y. Zhang, C.Y. Hu, Y. Pan, R. Pan, Y. L. Tang, B. Xu, N.Y. Gao, Enhanced coagulation and oxidation by the Mn(VII)-Fe(III)/peroxymonosulfate process: Performance and mechanisms, Water Res., 226 (2022) 119200.

[12] B. Liu, F. Qu, W. Chen, H. Liang, T. Wang, X. Cheng, H. Yu, G. Li, B. Van der Bruggen, Microcystis aeruginosa-laden water treatment using enhanced coagulation by persulfate/Fe(II), ozone and permanganate: Comparison of the simultaneous and successive oxidant dosing strategy, Water Res., 125 (2017) 72-80.

[13] J. Qi, H. Lan, S. Miao, Q. Xu, R. Liu, H. Liu, J. Qu, $KMnO_4$–Fe(II) pretreatment to enhance Microcystis aeruginosa removal by aluminum coagulation: Does it work after long distance transportation?, Water Res., 88 (2016) 127-134.

[14] B. Q. Yang, S. Rashid, N. Graham, W.Z. Yu, The impact of small organic molecules on Fe(II) coagulation: Facilitating vs. shielding mechanisms on charge transfer, Sep. Purif. Technol., 323 (2023) 124424.

[15] P. Li, W. Su, L. Zhong, H. Wang, X. Huang, T. Ruan, G. Jiang, Occurrence and ecological risk of alkylamine triazines in Chinese estuarine sediments: An emerging class of persistent, mobile, and toxic substances, Environ. Sci. Tech., 58 (2024) 6814-6824.

[16] S. Xiong, J. Fu, C. Dong, Z. Pei, R. Yang, Y. Li, Q. Zhang, G. Jiang, Bioaccumulation and trophodynamics of novel brominated flame retardants (NBFRs) in marine food webs from the arctic and antarctic regions, Environ. Sci. Tech., 58 (2024) 6804-6813.
[17] A. Peng, C. Wang, Z. Zhang, X. Jin, C. Gu, Z. Chen, Tetracycline photolysis revisited: Overlooked day-night succession of the parent compound and metabolites in natural surface waters and associated ecotoxicity, Water Res., 225 (2022) 119197.
[18] L. Yi, W. Zhang, Z. Chen, H. Li, Y. Lu, S. Tao, D. Zhu, Products from photolysis reactions of tetracycline mediated by clay and humic substance induce contrasting expressions of target resistance genes, Environ. Sci. Tech., 58 (2024) 13950-13960.
[19] N. Al-Jassim, M.I. Ansari, M. Harb, P.-Y. Hong, Removal of bacterial contaminants and antibiotic resistance genes by conventional wastewater treatment processes in Saudi Arabia: Is the treated wastewater safe to reuse for agricultural irrigation?, Water Res., 73 (2015) 277-290.
[20] A. Cai, J. Deng, M. Xu, T. Zhu, S. Zhou, J. Li, G. Wang, X. Li, Degradation of tetracycline by UV activated monochloramine process: Kinetics, degradation pathway, DBPs formation and toxicity assessment, Chem. Eng. J., 395 (2020) 125090.
[21] K. Guo, C. Yu, B. Gao, B. Liu, Z. Wang, Y. Wang, Q. Yue, Y. Gao, Intrinsic mechanism for the removal of antibiotic pollution by a dual coagulation process from the perspective of the interaction between NOM and antibiotic, Water Res., 244 (2023) 120483.
[22] C. Song, K.-X. Zhang, X.-J. Wang, S. Zhao, S.-G. Wang, Effects of natural organic matter on the photolysis of tetracycline in aquatic environment: Kinetics and mechanism, Chemosphere, 263 (2021) 128338.
[23] N. Chen, M. Huang, C. Liu, G. Fang, G. Liu, Z. Sun, D. Zhou, J. Gao, C. Gu, Transformation of tetracyclines induced by Fe(III)-bearing smectite clays under anoxic dark conditions, Water Res., 165 (2019) 114997.
[24] P.P. Zhang, Y.Y. Yang, X.G. Duan, S.B. Wang, Oxidative polymerization versus degradation of organic pollutants in heterogeneous catalytic persulfate chemistry, Water Res., 255 (2024) 121485.
[25] X. Peng, Z.Y. Fan, Q.Y. Wang, B.W. Yang, Recent advances on the role of high-valent metals formed during persulfate activation, Sep. Purif. Technol., 345 (2024) 127365.
[26] J.J. Zhang, W.X. Wang, W.R. Gao, Y.C. Cai, W. Wang, F.T. Tan, X.Y. Wang, X.L. Qiao, P.K. Wong, Great increasing N content in Fe-embedded carbon nanotubes to effectively activate persulfate for radical and nonradical degradation of organic contaminants, Sep. Purif. Technol., 330 (2024) 125429.
[27] X. Liu, S. Ding, P. Wang, Y. Hong, H. Zhao, W. Chu, Simultaneous mitigation of disinfection by-product formation and odor compounds by peroxide/Fe(II)-based process: Combination of oxidation and coagulation, Water Res., 201 (2021) 117327.
[28] X. Yang, L. Yao, Y. Wang, X. Zhang, P. Ren, Simultaneous removal of algae, microcystins and disinfection byproduct precursors by peroxymonosulfate (PMS)-enhanced Fe(III) coagulation, Chem. Eng. J., 445 (2022) 136689.
[29] M. L. Wang, Y.L. Wang, X.D. Jing, J.H. Xu, M. Li, Q. Xie, X.Y. Cai, Developments of efficient dithionite-zerovalent iron/persulfate systems with accelerated Fe(III)/Fe(II) cycle for PAHs removal in water and soils, Chem. Eng. J., 463 (2023).
[30] X. Li, N.J.D. Graham, W.S. Deng, M.J. Liu, T. Liu, W.Z. Yu, The formation of planar crystalline flocs of γ-FeOOH in Fe(II) coagulation and the influence of humic acid, Water Res., 185 (2020) 116250.
[31] L. Xu, Z. Zhang, N.J.D. Graham, W. Yu, Exploring the influence of aquatic phosphate on Fe floc dynamics in water treatment, Water Res., 262 (2024) 122146.

[32] Y. An, X. Li, Z. Liu, Y. Li, Z. Zhou, X. Liu, Constant oxidation of atrazine in Fe(III)/PDS system by enhancing Fe(III)/Fe(II) cycle with quinones: Reaction mechanism, degradation pathway and DFT calculation, Chemosphere, 317 (2023) 137883.
[33] H. Wang, H. Yao, P. Sun, D. Li, C. H. Huang, Transformation of tetracycline antibiotics and Fe(II) and Fe(III) species induced by their complexation, Environ. Sci. Tech., 50 (2016) 145-153.
[34] J. Yu, H. Xu, D. Wang, H. Sun, R. Jiao, Y. Liu, Z. Jin, S. Zhang, Variations in NOM during floc aging: Effect of typical Al-based coagulants and different particle sizes, Water Res., 218 (2022) 118486.
[35] X. Cheng, J. Wang, B. Yang, C. Wang, W. Chu, H. Guo, Reevaluation for UV photolysis of Fe(III) inducing tetracycline abatement: Overlooked significance of complexation-assistance in environmental fates of antibiotics, J. Hazard. Mater., 458 (2023) 131909.
[36] P. Zhang, X. Zhang, X. Zhao, G. Jing, Z. Zhou, Activation of peracetic acid with zero-valent iron for tetracycline abatement: The role of Fe(II) complexation with tetracycline, J. Hazard. Mater., 424 (2022) 127653.
[37] Z. Ma, H. Cheng, Insights into the photochemical mechanism of goethite: Roles of different types of surface hydroxyl groups in reactive oxygen species generation and Fe(III) reduction, Environ. Sci. Tech., 58 (2024) 14812-14822.
[38] J. He, C. Yang, Y. Deng, Z. Ouyang, Z. Huang, J. Yang, J. Zhou, C. He, Z. Dang, Mechanistic insights into the environmental fate of tetracycline affected by ferrihydrite: Adsorption versus degradation, Sci. Total Environ., 811 (2022) 152283.
[39] J. Li, L. Zhao, R. Zhang, H.H. Teng, L.P. Padhye, P. Sun, Transformation of tetracycline antibiotics with goethite: Mechanism, kinetic modeling and toxicity evaluation, Water Res., 199 (2021) 117196.
[40] W.S. Guo, S. Vigneswaran, H.H. Ngo, Effect of flocculation and/or adsorption as pretreatment on the critical flux of crossflow microfiltration, Desalination, 172 (2005) 53-62.
[41] Y. Chen, M. Zhang, L. Xie, Z. Wang, Q. Zhou, Molecular-weight-fractionation characteristics and coagulation behaviors of biorecalcitrant dissolved organic matter and colorants in cassava distillery wastewater, Ind. Eng. Chem. Res., 57 (2018) 4442-4451.
[42] J. Liu, C. Meng, X. Zhang, S. Wang, K. Duan, X. Li, Y. Hu, H. Cheng, Direct Z-scheme In_2O_3/AgI heterojunction with oxygen vacancies for efficient molecular oxygen activation and enhanced photocatalytic degradation of tetracycline, Chem. Eng. J., 466 (2023) 143319.
[43] A. Balakrishnan, M. Chinthala, A. Kumar, S. Rtimi, Construction of dual Z-scheme ternary carbon nitride homojunction pectin microspheres as a multifunctional photocatalyst for tetracycline degradation, H_2O_2 production, and N2 fixation, Chem. Eng. J., 496 (2024) 153899.
[44] X. Zou, B. Sun, L. Wang, H. Bai, X. Meng, C. Li, Z. Li, Enhanced photocatalytic degradation of tetracycline by SnS_2/Bi_2MoO_6-x heterojunction: Multi-electric field modulation through oxygen vacancies and Z-scheme charge transfer, Chem. Eng. J., 482 (2024) 148818.
[45] T. Zhang, S. Zhang, C. Wu, H. Zuo, Q. Yan, Novel La^{3+}/Sm^{3+} co-doped Bi_5O_7I with efficient visible-light photocatalytic activity for advanced treatment of wastewater: Internal mechanism, TC degradation pathway, and toxicity analysis, Chemosphere, 313 (2023) 137540.
[46] J. Liu, S. Li, C. Meng, J. Sun, X. Li, Y. Hu, H. Cheng, Visible-light induced tetracycline degradation catalyzed by dual Z-scheme $InVO_4$/$CuBi_2O_4$/$BiVO_4$ composites: The roles of oxygen vacancies and interfacial chemical bonds, Chem. Eng. J., 473 (2023) 145278.
[47] L. Wang, W. Wang, N. Graham, M.S. Siddique, H. Yang, W. Yu, Copper doped Fe-N-C as an excellent Fenton-like catalyst for membrane fouling mitigation against natural organic matters at neutral pH, J. Clean. Prod., 335 (2022) 130368.

[48] B. Yang, S. Rashid, N. Graham, G. Li, W. Yu, In-depth study of the removal of Mn(II) by Fe(VI) treatment and the profound influence of NOM on floc formation and properties, Water Res., 247 (2023) 120840.
[49] H. Yang, W. Xue, M. Liu, K. Yu, W. Yu, Carbon doped Fe_3O_4 peroxidase-like nanozyme for mitigating the membrane fouling by NOM at neutral pH, Water Res., 174 (2020) 115637.
[50] B. Yang, C. Wang, X. Cheng, Y. Zhang, W. Li, J. Wang, Z. Tian, W. Chu, G.V. Korshin, H. Guo, Interactions between the antibiotic tetracycline and humic acid: Examination of the binding sites, and effects of complexation on the oxidation of tetracycline, Water Res., 202 (2021) 117379.
[51] M.S. Siddique, Q. Song, X. Xiong, H. Fareed, N. Graham, W. Yu, Hydrolyzed polyacrylonitrile UF-membrane for surface and TAP water treatment: Influence on DBPs formation and removal, Chem. Eng. J., 471 (2023) 144314.
[52] X. Rong, W. Chen, Q. Huang, P. Cai, W. Liang, Pseudomonas putida adhesion to goethite: studied by equilibrium adsorption, SEM, FTIR and ITC, Colloids Surf., B, 80 (2010) 79-85.

631 **Figure Captions**

632 **Figure 1.** Flocculation index variation of (a) Fe(III) and Fe(II), (b) Fe(II) with PS, and (c)
633 flocculation index value of (a) and (b) at equilibration time, in $NaHCO_3$, HA, JM and JT (PS:
634 potassium persulfate, HA: humic acid, JM: Jingmi surface water, JT: JM with tetracycline
635 hydrochloride).

636 **Figure 2.** The intensity of removed substances and removal efficiency of (a) HA (0.1 mM
637 PS), (b) JM and (c) JT (0.01 mM to 1 mM PS), calculated from EEM (HA: humic acid, JM:
638 Jingmi surface water, JT: JM with tetracycline hydrochloride, EEM: the excitation and
639 emission matrix fluorescence spectra, EEM partition I: protein I, II: protein II, III: fulvic acid,
640 IV: microbial metabolites, V: humic acid, PS: potassium persulfate).

641 **Figure 3.** Integral area removal efficiency of different molecular weight of (a) HA, (b) JM
642 and (c1) JT, calculated from SEC, (c2) removal efficiency of JT calculated from UV
643 absorbance, (d) enhanced removal efficiency of HA and JM by PS (HA: humic acid, JM:
644 Jingmi surface water, JT: JM with tetracycline hydrochloride, SEC: size exclusion
645 chromatography, SEC peak of HA: I(7052-50000), II(5359-7052), III(3547-5359), peak of
646 JM: I(5648-13145), II(3811-5648), peak of JT: I(3031-6773), II(2061-3031), PS: potassium
647 persulfate).

648 **Figure 4.** (a) ESR of Fe in the absence/presence of PS, (b) LC-MS intensity and
649 reduced/increased intensity of JT raw water and treated water (ESR: electron spin resonance,
650 PS: potassium persulfate, LC-MS: liquid chromatography-tandem mass spectrometry, JT:
651 Jingmi surface water with tetracycline hydrochloride).

652 **Figure 5.** TEM, HAADF, SEM, HRTEM images and schematic diagrams of flocs (a) Fe(II),
653 (b) Fe(II) with PS of 0.1 mM and (c) Fe(III) in JM (TEM: transmission electron microscopy,
654 HAADF: high angle annular dark field, SEM: scanning electron microscope, HRTEM: high-
655 resolution TEM, PS: potassium persulfate, JM: Jingmi surface water).

Figure 6. FTIR spectra of flocs in (a) $NaHCO_3$, HA and JM, asynchronous (b) and (c) synchronous 2D-COS map of Fe(II) flocs with PS, red colors represent positive intensities, blue colors represent negative intensities (FTIR: Fourier transform infrared spectrometry, HA: humic acid, JM: Jingmi surface water, 2D-COS: two-dimensional correlation spectroscopy, PS: potassium persulfate).

Figure 7. The Fe floc performance on the removal of (a) NOM, and (b) TC (PS: potassium persulfate, NOM: natural organic matter, TC: tetracycline).

Revised Figure
Click here to access/download;Figure;Revised Figure 1_clean version.docx

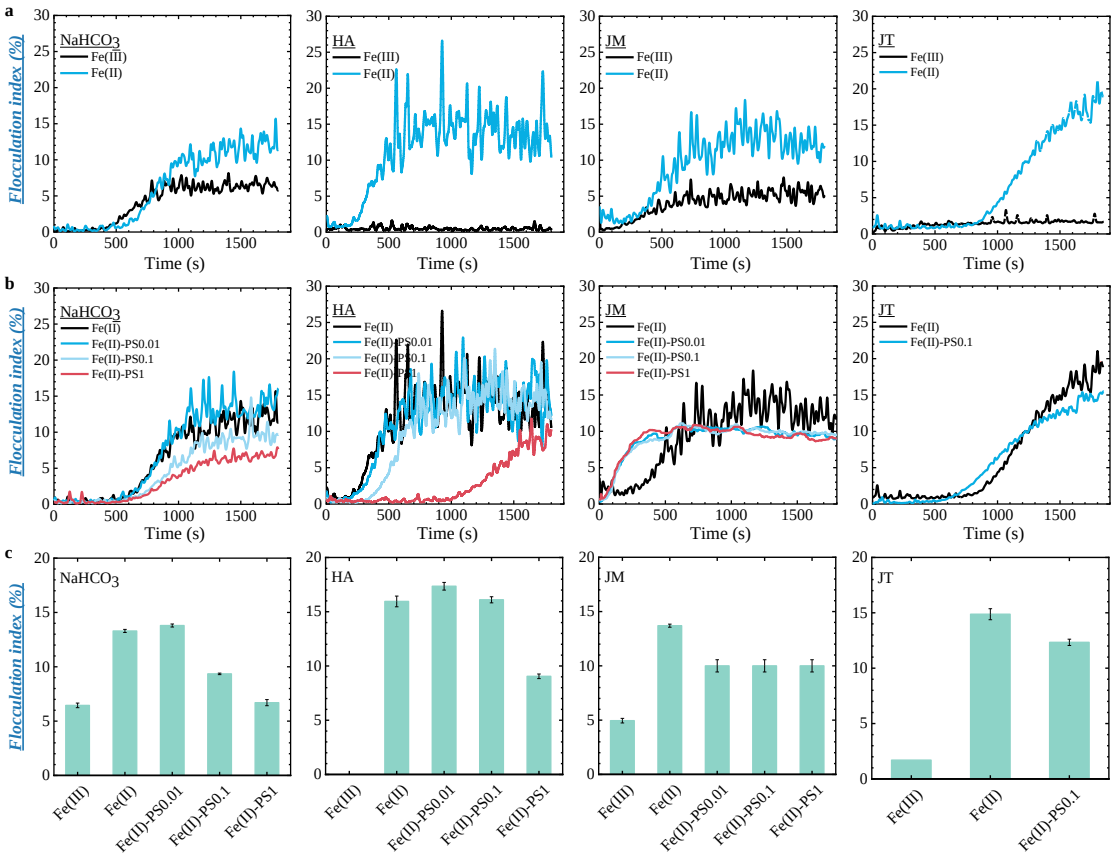


Figure 1. Flocculation index variation of (a) Fe(III) and Fe(II), (b) Fe(II) with PS, and (c) flocculation index value of (a) and (b) at equilibration time, in $NaHCO_3$, HA, JM and JT (PS: potassium persulfate, HA: humic acid, JM: Jingmi surface water, JT: JM with tetracycline hydrochloride).

Click here to access/download;Figure;Figure 2.docx

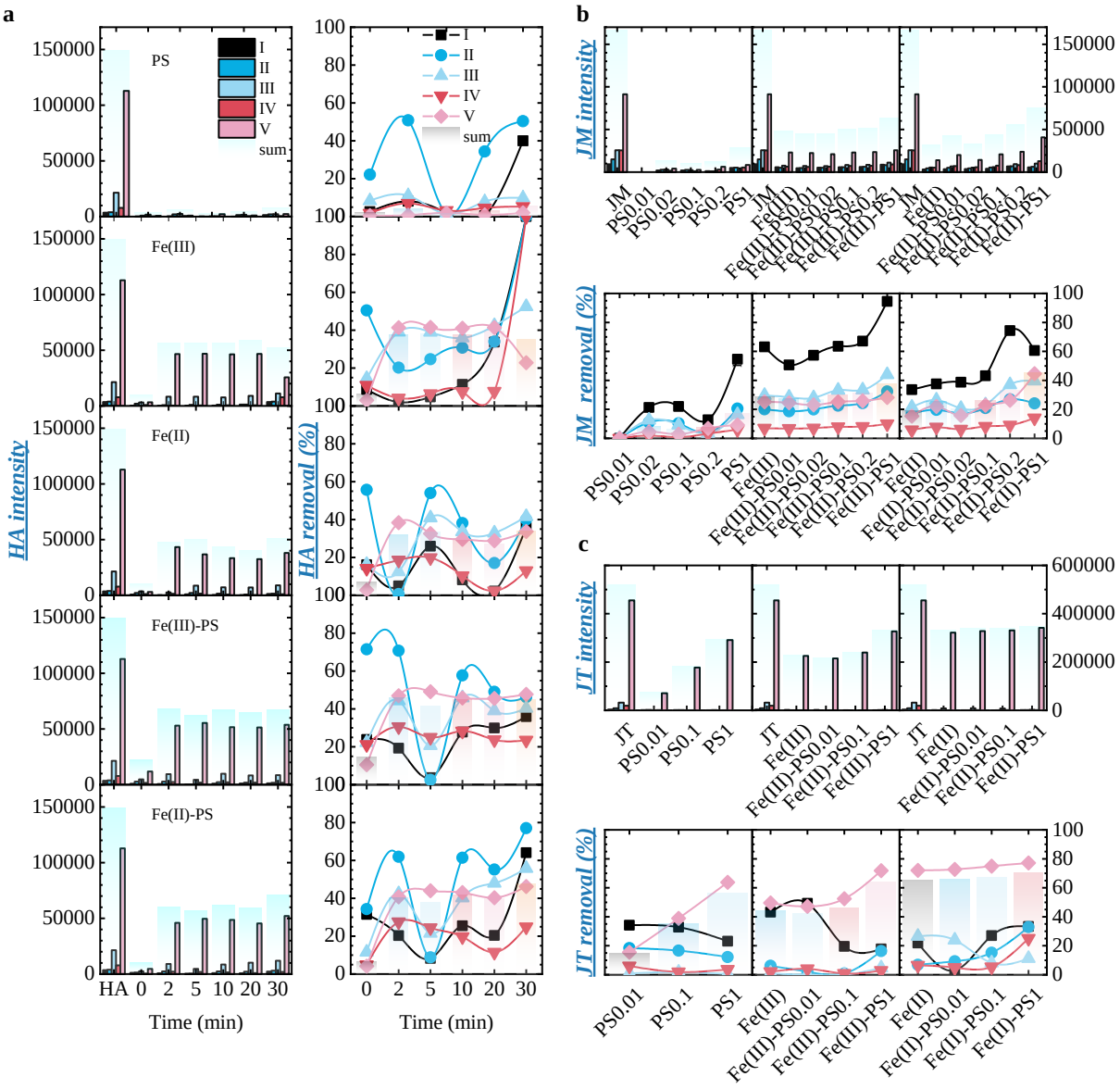


Figure 2. The intensity of removed substances and removal efficiency of (a) HA (0.1 mM PS), (b) JM and (c) JT (0.01 mM to 1 mM PS), calculated from EEM (HA: humic acid, JM: Jingmi surface water, JT: JM with tetracycline hydrochloride, EEM: the excitation and emission matrix fluorescence spectra, EEM partition I: protein I, II: protein II, III: fulvic acid, IV: microbial metabolites, V: humic acid, PS: potassium persulfate).

Click here to access/download;Figure;Figure 3.docx

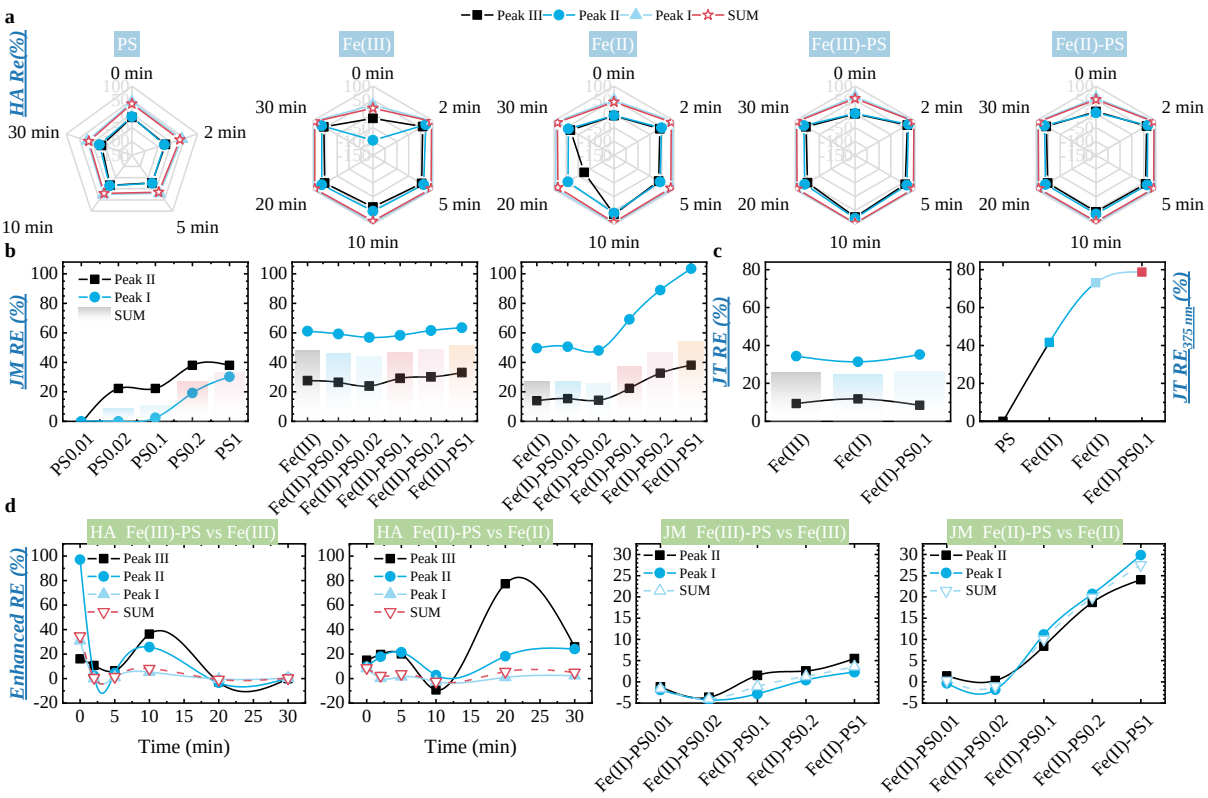


Figure 3. Integral area removal efficiency of different molecular weight of (a) HA, (b) JM and (c1) JT, calculated from SEC, (c2) removal efficiency of JT calculated from UV absorbance, (d) enhanced removal efficiency of HA and JM by PS (HA: humic acid, JM: Jingmi surface water, JT: JM with tetracycline hydrochloride, SEC: size exclusion chromatography, SEC peak of HA: I(7052-50000), II(5359-7052), III(3547-5359), peak of JM: I(5648-13145), II(3811-5648), peak of JT: I(3031-6773), II(2061-3031), PS: potassium persulfate).

Click here to access/download;Figure;Figure 4.docx

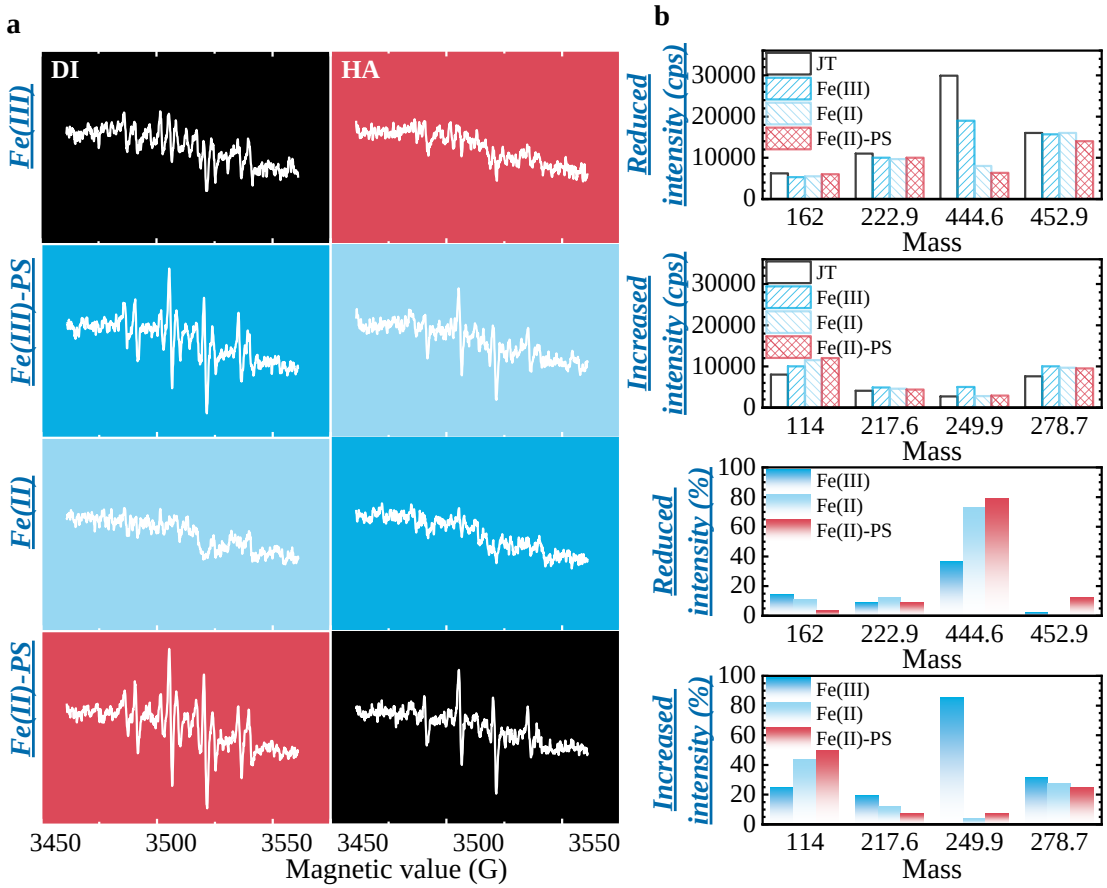


Figure 4. (a) ESR of Fe in the absence/presence of PS, (b) LC-MS intensity and reduced/increased intensity of JT raw water and treated water (ESR: electron spin resonance, PS: potassium persulfate, LC-MS: liquid chromatography-tandem mass spectrometry, JT: Jingmi surface water with tetracycline hydrochloride).

Click here to access/download;Figure;Figure 5.docx

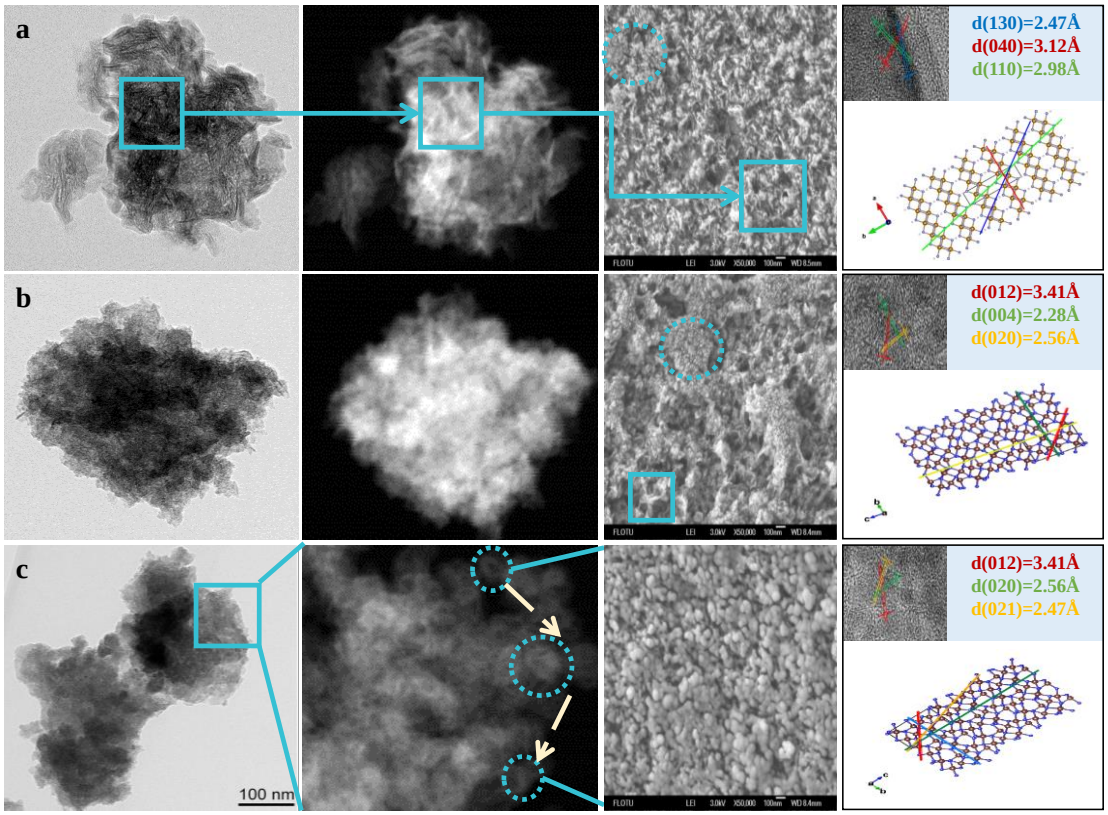


Figure 5. TEM, HAADF, SEM, HRTEM images and schematic diagrams of flocs (a) Fe(II), (b) Fe(II) with PS of 0.1 mM and (c) Fe(III) in JM (TEM: transmission electron microscopy, HAADF: high angle annular dark field, SEM: scanning electron microscope, HRTEM: high-resolution TEM, PS: potassium persulfate, JM: Jingmi surface water).

Click here to access/download;Figure;Revised Figure 6_clean version.docx

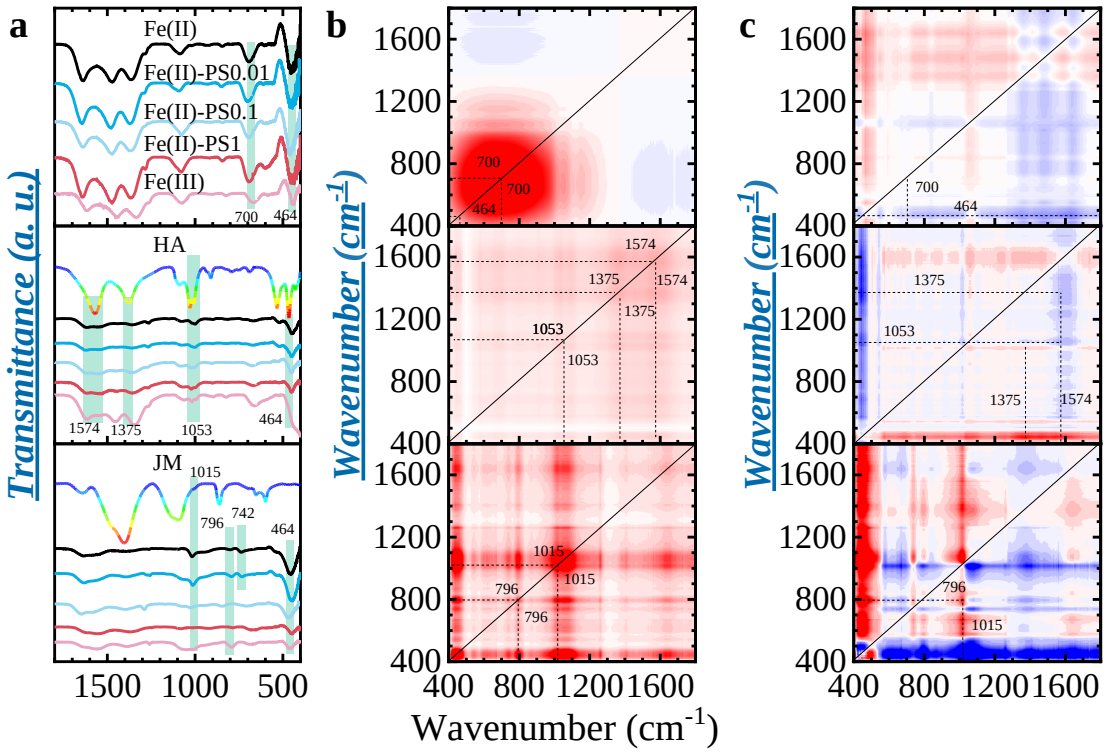


Figure 6. FTIR spectra of flocs in (a) $NaHCO_3$, HA and JM, asynchronous (b) and (c) synchronous 2D-COS map of Fe(II) flocs with PS, red colors represent positive intensities, blue colors represent negative intensities (FTIR: Fourier transform infrared spectrometry, HA: humic acid, JM: Jingmi surface water, 2D-COS: two-dimensional correlation spectroscopy, PS: potassium persulfate).

Click here to access/download;Figure;Figure 7.docx

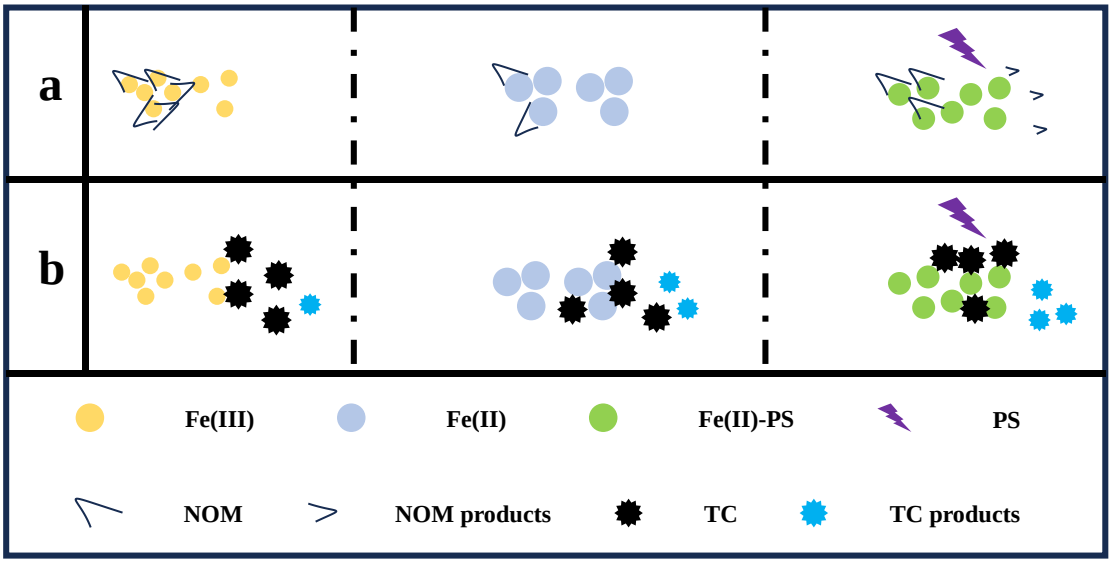


Figure 7. The Fe floc performance on the removal of (a) NOM, and (b) TC (PS: potassium persulfate, NOM: natural organic matter, TC: tetracycline).